Three-dimensional dispersion entropy for uterine fibroid texture quantification and post-embolization evaluation

Delphine Lebret, Andreia S. Gaudencio, Mirvana Hilal, Sonia Saib, Rakelle Haidar, Michel Nonent, Anne Humeau-Heurtier

Three-dimensional dispersion entropy for uterine fibroid texture quantification and post-embolization evaluation*

Delphine Lebret[a,b,*], Andreia S. Gaudêncio[a,c], Mirvana Hilal[a], Sonia Saib[d], Rakelle Haidar[a], Michel Nonent[d] and Anne Humeau-Heurtier[a]

[a] Univ Angers, LARIS, SFR MATHSTIC, F-49000 Angers, France.
[b] Polytech Grenoble, Grenoble INP - Grenoble Alpes University, France.
[c] LIBPhys, University of Coimbra, Portugal.
[d] CHRU La Cavale Blanche, Brest, France.

ARTICLE INFO

Keywords:
entropy
magnetic resonance imaging
multiscale analysis
quality of life
texture
uterine fibroid embolization

ABSTRACT

Background and Objective: Uterine fibroids are benign tumors that could lead to symptoms complicating a patient's daily life. Those fibroids can be treated using uterine fibroid embolization (UFE), an effective non-surgical procedure. However, objectively quantifying the benefits of such a procedure, and the patient's quality of life, is rather challenging. **Methods**: With a novel multiscale three-dimensional (3D) entropy-based texture analysis, the multiscale 3D dispersion entropy ($MDispEn_{3D}$), this work aims to objectively quantify the evolution – after UFE – of patients' health in terms of quality of life, symptoms severity, and sexual function. For this purpose, clinical data and magnetic resonance imaging (MRI) scans of fibroids are analyzed before UFE (D0), ten days after (D10), and six months after (M6). **Results**: An inverse correlation is observed between $MDispEn_{3D}$ entropy values and both size and volume of fibroids. An inverse correlation is also observed between $MDispEn_{3D}$ at M6 and the scores of symptoms severity. Moreover, the patient age is found to be related to the relative difference of $DispEn_{3D}$ and $MDispEn_{3D}$ values, between D0 and M6, translating into an increasing entropy value. Furthermore, we show that history of fibroma plays a role in determining the obtained $DispEn_{3D}$ values at D0. Finally, we observe that the lower $MDispEn_{3D}$ values at D0, the larger the size of the fibroid at M6. **Conclusions**: The proposed $MDispEn_{3D}$ method – by quantifying fibroid texture – could assist the medical doctors in the prognosis of uterine fibroids and the patients' quality of life assessment post-UFE. It could therefore favor the choice of this treatment compared to other more invasive surgical treatments.

1. Introduction

Uterine fibroids, also called leiomyomas, are benign tumors that grow in the uterus. Twenty to thirty percent (20%-30%) of women in their childbearing years are affected by this condition, half of them being asymptomatic [1, 2]. For the other half, symptoms degrade the quality of life, the sexual function, and can cause pelvic pain and heaviness, amenorrhea, menometrorrhagia, compression of nearby organs, infertility or even early miscarriage [1].

Fibroids are composed of muscular and fibrous tissues. Their location can be subserous, interstitial/intramural, or submucosal/intracavitary (International Federation of Gynaecology and Obstetrics classification) [3]. Their type can be non-degenerated or degenerated, non-degenerated oedematous, hypercellular, mixoid/cystic or "red" degeneration, and adenomyoma [4]. Moreover, the incidence of uterine fibroids is higher for women of dark skin, with a higher number of fibroids present and being of a larger size, and associated with more invalidating symptoms. There are also other dispositions to uterine fibroids such as diabetes, family history, nulliparity, obesity, and hypertension. So far, no genetic cause has been found for common uterine fibroids. However, for rare uterine fibroids, such as multiple cutaneous and uterine leiomyomatosis, their occurrence has been attributed to genes encoding the mitochondrial enzyme, fumarate hydratase. In addition, it has been shown that the ovarian steroids estrogen and progestin, growth factors, angiogenesis, and apoptosis processes are the primary regulators of fibroid growth [1, 2].

Patients suffering from uterine fibroids can use medication to reduce the symptoms or limit the evolution of the fibroid. Surgery is also possible to remove the fibroid (myomectomy) or the uterus (hysterectomy). Other procedures, such as uterine fibroid embolization (UFE), can also be proposed to either reduce or destroy the fibroid. UFE is a minimally invasive procedure in which the radiologist injects microspheres of hydrogel into the arteries that feed the fibroid. The goal is to block the fibroid influx. Since the 1990's, this procedure is used as an alternative to myomectomies and hysterectomies as it is safer and is associated with less complications [5].

In order to evaluate the benefits of UFE, surveys can be proposed to patients. These surveys are composed of scales and questions where the patients have to answer on a *Likert* scale. The latter includes five different answers that define the degree of strength, agreement, and frequency according to the questions asked (e.g., very high, high, medium, low, very low, or nonexistent). The answers are studied as ordinal variables. Spies et al. [6] proposed the so-called Uterine

* Funding sources here.
*Corresponding author
delphine.lbt49@gmail.com (D. Lebret)
ORCID(s):

Fibroid Symptom and Quality Of Life (UFS-QOL) survey to determine a severity of symptoms (SSS) score and a quality of life (HRQL) score. A high SSS score indicates severe symptoms, while a high HRQL score indicates a good quality of life. From these scores, it has been reported that patients who undergo UFE have a significant change in their quality of life and symptoms severity 3 months after embolization [6]. Female sexual function index (FSFI) has also been proposed in [7]. FSFI evaluates the sexual function of women. It is composed of sub-scores such as desire, arousal, lubrication, orgasm, satisfaction, and pain. A high FSFI score represents good sexual function. However, a score below 26.55 indicates sexual dysfunction [7].

Although these surveys provide important information, once the UFE procedure is performed, it is still difficult for radiologists to *objectively quantify* the evolution of patients' health and, thus, evaluate the patients' well being after embolization. In order to overcome this drawback, we herein propose, first, to quantify MRI fibroid texture through a novel multiscale tridimensional entropy-based algorithm. Texture of an image is related to the structure of its patterns. It has recently been shown that entropy-based measures can lead to interesting results for texture quantification [8, 9, 10, 11, 12] To the best of our knowledge, only two algorithms have been proposed for the analysis of three-dimensional data: the approximate entropy (ApEn3D) [13] and the fuzzy entropy (FuzEn3D) [14, 15]. In this work, we introduce the multiscale three-dimensional dispersion entropy (MDispEn$_{3D}$) to evaluate the irregularity and complexity of uterine fibroids towards an assisted diagnosis. Second, in this study we also propose to study the relation between the entropy-based texture and patient quality of life as determined through the two above-mentioned surveys. Our results could therefore help the medical doctors in improving the patients' quality of life and performing better prognosis after UFE procedure.

The rest of the paper is organized as follows: the Materials and Methods section introduces the new multiscale 3D entropy-based algorithm, the synthetic data proposed for the algorithm validation, and the clinical data used. We also present the statistical tests performed. The results are detailed and analyzed in the Results and Discussion section. We finally end with a conclusion.

2. Materials and methods

2.1. Multiscale three-dimensional dispersion entropy

To objectively quantify the evolution of patient health after UFE, we first propose to quantify the texture of volumetric MRI data. For this purpose, we introduce the extension of the dispersion entropy (DispEn) [16] algorithm to 3D data (DispEn$_{3D}$). Moreover, we also propose a multiscale approach for DispEn$_{3D}$ (MDispEn$_{3D}$).

The DispEn algorithm [16] quantifies the irregularity of a signal by first mapping the signal into several classes (c classes). The mapping procedure can be performed using linear or nonlinear techniques. For this purpose, the first step is to assign the signal, $\mathbf{x}$, elements with a value between 0 and 1, obtaining $\mathbf{y}$. Then, each element of $\mathbf{y}$ is assigned an integer (from 1 to c). Once each element has its class defined, several vectors of m elements are obtained, where m is the embedding dimension. These vectors are called templates or embedding vectors and are basically a group of samples of the mapped signal with the assigned classes. Each of these templates are converted to dispersion patterns. Afterwards, the probability of each possible dispersion pattern is calculated. The final step is to obtain the entropy value using the Shannon's definition for these probability values [16]. The three-dimensional version, DispEn$_{3D}$, is very similar to DispEn, where the main differences are that the analysed data, $\mathbf{U}$, has three-dimensions, and therefore, the templates are no longer vectors but three-dimensional structures, and the mapped data will also be a volume, $\mathbf{Y}$.

Consider a volume $\mathbf{U}$ of dimensions $H \times W \times L$, where H represents the height, W represents the width, and L the length, with its elements being $u_{i,j,k}$ for $1 \leq i \leq H$, $1 \leq j \leq W$, and $1 \leq k \leq L$.

First, each element $u_{i,j,k}$ is mapped with integers from 1 to c classes. This procedure can be performed using linear or nonlinear approaches. To obtain DispEn$_{3D}$, the normal cumulative distribution function (NCDF) is used to perform the mapping procedure. Even though linear mapping can be fast, for a distribution of $\mathbf{U}$ where the extreme values (maximum/minimum) are considerably larger than the median or mean value, the mapping results in very few classes. In addition, some natural processes are known for having a sigmoid-based behavior [16, 17]. Therefore, the NCDF is used to map the volume $\mathbf{U}$ to the new volume $\mathbf{Y}$. The elements $y_{i,j,k}$ of $\mathbf{Y}$ are obtained as follows:

$$y_{i,j,k} = \frac{1}{\sigma\sqrt{(2\pi)}} \int_{-\infty}^{u_{i,j,k}} \exp^{\frac{-(t-\mu)^2}{2\sigma^2}} dt \,, \tag{1}$$

where μ is the mean value of $\mathbf{U}$, σ is the standard deviation (SD) of $\mathbf{U}$, and $y_{i,j,k}$ is the element of the mapped volume $\mathbf{Y}$ assuming a value between 0 and 1.

Afterwards, each $y_{i,j,k}$ is assigned to an integer value between 1 and c, obtaining the elements of $\mathbf{Z}$ according to the following procedure:

$$z^c_{i,j,k} = round(c \times y_{i,j,k} + 0.5) \,. \tag{2}$$

Then, the templates, $z^{c,m}(p,q,r)$, are obtained using the embedding dimension vector, $\mathbf{m} = [m_H, m_W, m_L]$, as follows:

$$\begin{aligned} z^{c,m}(p,q,r) = \{ z^c(p+\alpha, q+\beta, r+\gamma) \} \,, \\ 1 \leq \alpha \leq m_H - 1, \\ 1 \leq \beta \leq m_W - 1, \\ 1 \leq \gamma \leq m_H - 1 \,, \end{aligned} \tag{3}$$

with $1 \leq p \leq H - m_H - 1$, $1 \leq q \leq W - m_W - 1$, and $1 \leq r \leq L - m_L - 1$. Therefore, the template can be defined

as a sub-sample of the volume. Afterwards, each template $z^{c,m}(p,q,r)$ is mapped to a dispersion pattern $\pi_{v_0,v_1,\ldots,v_n}$ with $n = m_H \times m_W \times m_L - 1$, $v_0 = z^c(p,q,r)$, $v_1 = z^c(p+1,q,r)$, and $v_n = z^c(p+m_H-1, q+m_W-1, r+m_L-1)$.

The number of possible dispersion patterns, n_z, for each template $z^{c,m}(p,q,r)$ is $n_z = c^{m_H \times m_W \times m_L}$. This number emerges due to the fact that the number of elements of a template is $m_H \times m_W \times m_L$, and each element is mapped as an integer number between 1 and c. The number of possible embedded dispersion patterns is $N_m = (H - m_H + 1) \times (W - m_W + 1) \times (L - m_L + 1)$.

For each potential dispersion patterns $\pi_{v_0,v_1,\ldots,v_n}$, we obtain the relative frequency as follows:

$$p(\pi_{v_0,\ldots,v_n}) = \frac{\#\{p,q,r | z^{m,c}(p,q,r) \text{ has type } \pi_{v_0,\ldots,v_n}\}}{N_m}, \quad (4)$$

with $p \leq H - m_H - 1$, $q \leq W - m_W - 1$, and $r \leq L - m_L - 1$. The probability $p(\pi_{v_0,\ldots,v_n})$ corresponds to the number of dispersion patterns of $\pi_{v_0,v_1,\ldots,v_n}$ for its corresponding template $z^{m,c}(p,q,r)$ within the total number of possible embedded templates N_m.

Then, using the Shannon's entropy definition, DispEn_{3D} is obtained as:

$$\text{DispEn}_{3D}(\mathbf{U}, m, c) = -\sum_{\pi=1}^{n_z} p(\pi_{v_0,\ldots,v_n}) \times \ln(p(\pi_{v_0,\ldots,v_n})) . \quad (5)$$

As an illustration, consider the volume in Figure 1 with 4 voxels height, 3 voxels width, and 2 voxels length. The values of each $H \times W$ matrix within the length of the volume are also shown in Figure 1. According to the DispEn_{3D} algorithm, the first step is to obtain the volume $\mathbf{Y}$ based on the NCDF mapping (Figure 2). Then, each voxel is rounded according to Equation 2. In this case, if we define the number of classes as $c = 3$, this leads to the volume shown in Figure 3. Then, we have to create the templates. For the purposes of this example, we define the embedding dimension as $\mathbf{m} = [2,2,2]$. In Figure 4, we can observe that the first template $z^{c,m}(1,1,1)$ corresponds to the voxels in pink and the second, $z^{c,m}(1,2,1)$, corresponds to the blue ones.

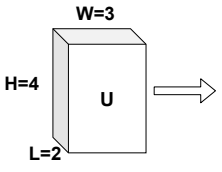

0.1	0.2	0.4
3.2	2.4	1.8
2.6	0.5	0.3
0.1	0.6	0.7

0.7	0.8	1.1
1.4	3.6	1.2
0.9	0.3	2.4
3.3	2.1	0.8

Figure 1: Example of a volume **U** with $H = 4$, $W = 3$, and $L = 2$ (left), with the corresponding values for each layer within the length of the volume (right).

The number of possible templates for the established $\mathbf{m}$ is $N_m = (4-2+1) \times (3-2+1) \times (2-2+1) = 6$.

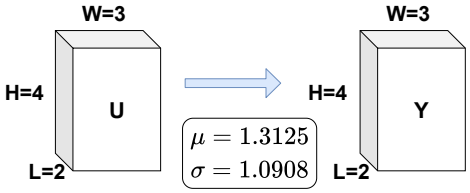

0.1332	0.1539	0.2014
0.9582	0.8406	0.6725
0.8811	0.2282	0.1766
0.1332	0.22568	0.2872

0.2872	0.3192	0.4228
0.5320	0.9820	0.4589
0.3527	0.1766	0.8406
0.9650	0.7648	0.3192

Figure 2: Volume **Y** (right at the top) obtained after the mapping procedure of volume **U** (presented in Figure 1), with mean and SD values of $\mu = 1.3125$ and $\sigma = 1.0908$, respectively, and the corresponding values for each layer within the length of **Y** (bottom).

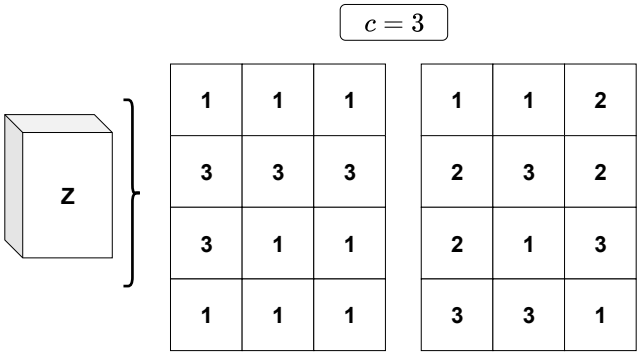

1	1	1
3	3	3
3	1	1
1	1	1

1	1	2
2	3	2
2	1	3
3	3	1

Figure 3: Volume **Z** obtained after the rounding operation of the elements of **Y** shown in Figure 2, for $c = 3$.

In this case, none of the dispersion patterns obtained repeats itself. Therefore, the probability of each pattern is $1/6$. After applying the Shannon definition, for this example, we verify that the entropy value using DispEn_{3D} is 1.7918.

Costa et al. [18] suggested the use of a multiscale analysis to evaluate the irregularity of biomedical systems through multiple temporal scales. This approach, originally applied to signals, is based on a coarse-graining procedure where the signal is down-sampled using an averaging method for multiple scale factors (τ). By extending the original procedure to three-dimensions, for a volume $\mathbf{U}$, the new coarse-grained volume $\mathbf{Y}^{(\tau)}$ is obtained as follows:

$$\mathbf{Y}_{i,j,k}{}^{(\tau)} = \frac{1}{\tau^3} \sum_{\substack{l=(i-1)\tau+1 \\ m=(j-1)\tau+1 \\ n=(k-1)\tau+1}}^{\substack{k\tau \\ j\tau \\ i\tau}} \mathbf{U}_{l,m,n} , \quad (6)$$

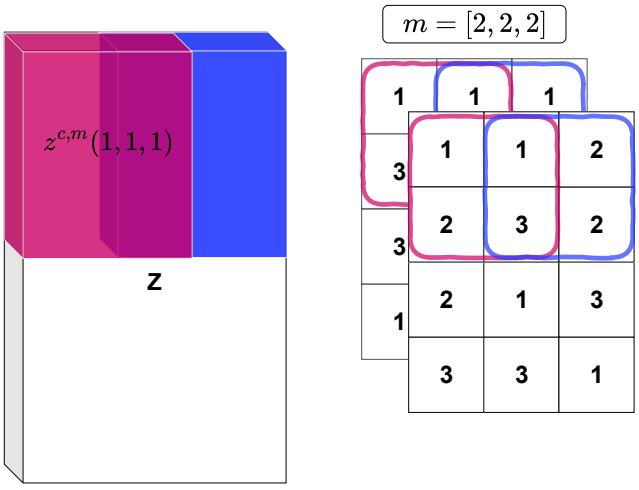

Figure 4: Representation of the embedded templates for $\mathbf{m} = [2,2,2]$ of the volume $\mathbf{Z}$.

where τ is the scale factor, determining the rate of down-sampling, $1 \leq l \leq H/\tau$, $1 \leq m \leq W/\tau$, and $1 \leq n \leq L/\tau$, and the volume $\mathbf{Y}^{(\tau)}$ has $\frac{H}{\tau} \times \frac{W}{\tau} \times \frac{L}{\tau}$ voxels. For example, if a volume $\mathbf{U}$ has 100×100×100 voxels, for $\tau = 1$, $\mathbf{Y}^{(1)} = \mathbf{U}$, for $\tau = 2$, the volume $\mathbf{Y}^{(2)}$ will have half of the length, half of the width, and half of the height, having therefore, $50 \times 50 \times 50$ voxels, and for $\tau = 3$, $\mathbf{Y}^{(3)}$ will have a third of the length, a third of the width, and a third of the height, *i.e.*, $33 \times 33 \times 33$ voxels, and so on.

When using a multiscale approach, several τ values are used, leading to several coarse-grained versions of the original volume. Then, the entropy measure (in this case DispEn_{3D}) is applied to each coarse-grained volume, leading to the multiscale approach (in this case, MDispEn_{3D}) to evaluate the complexity of a biomedical data. The maximum scale factor determines the size of the smallest down-sampled volume. Due to the size of our data, the maximum τ value was chosen equal to 6. For our analysis, the DispEn_{3D} entropy values were thus analyed for $1 \leq \tau \leq 6$. Besides, a new variable θ was defined based on the sum of these MDispEn_{3D} values:

$$\theta = \sum_{\tau=1}^{6} MDispEn_{3D}(\tau), \tag{7}$$

where $MDispEn3D(\tau)$ corresponds to the multiscale entropy value obtained for the scale factor τ using DispEn_{3D} as the entropy measure. The algorithms were excuted using MATLAB®.

2.2. Validation tests

We performed several tests for the proposed algorithms to validate their ability on identifying increasing irregularity degrees and verify their proper behavior with 3D data. DispEn_{3D} was tested on different cubes of dimensions $256 \times 256 \times 256$ voxels. These volumes are composed of images taken from [19]. The first group of synthetic textures was composed of periodic images as shown in Figure 5 (a), (b), and (c), while the second group was composed of non-periodic images as shown in Figure 5 (d), (e), and (f). An algorithm generates these textures using a deterministic search process where each region of the periodic texture is equivalent to that of the non-periodic texture [20]. This algorithm is based on Markov random field texture models. To compute DispEn_{3D} values, the parameters were set as $c = 5$, and $\mathbf{m} = [2,2,2]$. These parameters were used previously for 1D data in [16, 21]. This test will allow to illustrate if the DispEn_{3D} algorithm is able to differentiate texture behaviors.

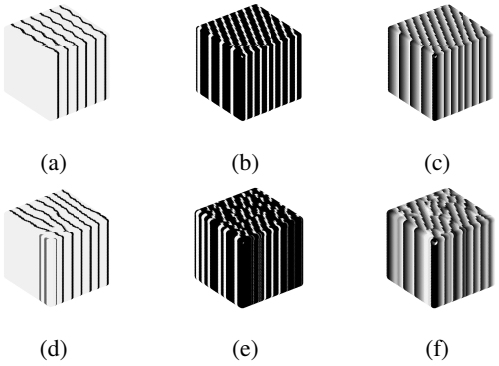

Figure 5: Volumes of 256×256×256 voxels presenting periodic textures (a), (b), and (c), and their non-periodic textures (d), (e), and (f) based on the textures of [22].

2.3. Clinical data

The magnetic resonance imaging (MRI) scans were obtained from 42 patients who went through UFE (at 3 time instances for the follow-up), in the Centre Hospitalier Regional Universitaire (CHRU) La Cavale Blanche and the Polyclinique Keraudren, both in Brest, between 2018 and 2020. Consent was obtained from the patients and the work has been approved by the ethical committee. The study of MRI scans was performed for sagittal T2 scans without gadolinium as recommended by the medical doctors. The average age of the patients was 45 +/- 9 years, that is goes back to the most common age of the onset of fibroids [1, 2]. This study included the UFS-QOL and FSFI surveys. The patients had to complete these surveys at 3 time instances: the day of the UFE procedure (D0), after 10 days (D10), and after six months (M6). The protocol was carried out by an experienced radiologist (Pr. M.N.). The patients underwent the procedure under local anesthesia. The embolization was realized with Embosphere®. The definition of the region of interest (ROI) was performed by Dr. S.S., a radiology intern; the volume of the fibroid and the apparent diffusion coefficient (ADC) were computed. ADC is related to the degree of water diffusion in tissues [23].

Several variables were studied, including clinical and image-based features. The clinical data included the following: age, body mass index (BMI), gestiture, parity, number of spontaneous miscarriages, presence of a previous fibroid,

type of contraception used, treatment taken by the patient before embolization (D0), and the scores obtained from the surveys (FSFI, SSS, and HRQL) at D0 and M6. From the fibroid, characteristics like volume and ADC were also considered at D0, D10, and M6. These variables were defined as being related either to the appearance of a fibroid or its evolution.

The MRI scans were evaluated using MDispEn_{3D}. The size of the main fibroid was identified with the medical doctors. To determine the volume to process, first a square containing the ROI was determined by the radiologist and defined on an equal volume regardless of the MRI acquisition instant for each patient (see Figures 6 and 7). Then, the number of processed images (z-dimension) was considered to be the minimum number of images composing each patient's MRI scans (D0, D10, M6). The smallest volume of interest (VOI) considered in the study had a dimension of $46 \times 46 \times 28$ voxels and the largest had a dimension of $233 \times 233 \times 28$ voxels. The size of fibroid was obtained using the major axis of the fibroid (see Figure 6).

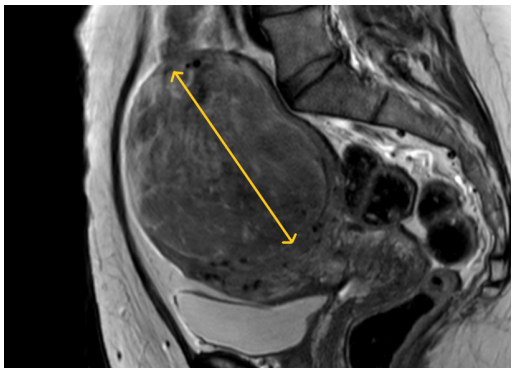

Figure 6: MRI scan of a patient with the definition of the size of the fibroid (yellow arrow).

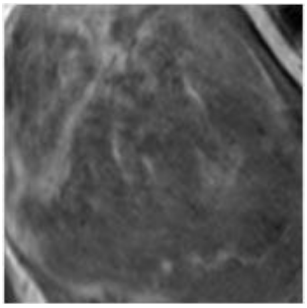

Figure 7: Squared ROI defined according to the MRI shown in Figure 6.

The ROI was then normalized to obtain a comparable average gray level among the MRI scans. The normalization procedure was performed as follows:

$$\mathbf{V}_{norm} = \frac{\mathbf{V} - \min(\mathbf{V})}{\max(\mathbf{V}) - \min(\mathbf{V})}, \tag{8}$$

where $\mathbf{V}$ is the VOI containing the original ROI selected by the radiologist of a patient at one time period (D0, D10, or M6), $\min(\mathbf{V})$ corresponds to the minimum value of $\mathbf{V}$, and $\max(\mathbf{V})$ to the maximum value of $\mathbf{V}$.

The entropy of the VOI was calculated using the MDispEn_{3D} algorithm, with the following parameters: number of classes $c = 5$, embedding dimension $\mathbf{m} = [2, 2, 2]$, and the maximum τ value was chosen equal to 6. We have chosen the same parameters (number of classes, embedding dimensions, and τ) as in the texture validation test, recommended for 1D data [16, 21]

2.4. Statistical analysis

When analyzing entropy curves, all of the 42 patients were included in the analysis. When analyzing the survey answers and the entropy for correlation analysis, we only used 34 patients as 8 of them did not complete the surveys. After obtaining the 30 variables from the surveys, a descriptive statistical analysis was performed using the R® software. The minimum, maximum, and average values of each variable were considered. In addition, the normality and variance of these variables were verified using graphics. The normality assessment was performed using the *Shapiro-Wilk* test with a statistical significance of $\alpha = 0.05$.

We define the relative difference (RD) between D0 and M6 as:

$$RD_1(X) = \frac{X_{M6} - X_{D0}}{X_{D0}}, \tag{9}$$

where X is the variable under study, X_{D0} corresponds to the variable X before the embolization at D0, and X_{M6} is the variable X six months after embolization.

Similarly, we also define the relative difference of a variable between D0 and D10 as:

$$RD_2(X) = \frac{X_{D10} - X_{D0}}{X_{D0}}. \tag{10}$$

For all the statistical tests, the threshold of statistical significance was $\alpha = 0.05$.

The identification of a relationship between several continuous quantitative variables was performed using the *Pearson*'s correlation coefficient (parametric) test or the *Spearman*'s correlation coefficient (non-parametric) test. For a p-value lower than the significance level, the correlation was accepted, rejecting the null hypothesis, and the correlation coefficients were retained. Then, the explanatory variables with normal distribution were studied using linear regression. For the variables that did not follow the normal distribution, a logarithmic transformation or using Box-Cox was used.

The variables with a normal distribution were used to explain the difference of the mean values between two samples. When the samples had the same variance values, the Student's test was performed. Otherwise, the *Welch*'s test was implemented. Through the *Fisher*'s test, the equality of variance between two samples was also verified.

Table 1
$DispEn_{3D}$ values on the volumes composed by periodic textures (a), (b), and (c), and non-periodic textures (d), (e), and (f) shown in Figure 5.

Texture (a)	Texture (b)	Texture (c)
1.07	1.13	2.34
Texture (d)	**Texture (e)**	**Texture (f)**
1.14	1.20	2.58

When testing more than two samples, the equality of variances was analyzed. The mean values were compared with the ANOVA (parametric) test or the *Kruskal-Wallis* (non-parametric) test. In case of a significant result for the ANOVA test, when having a control group, we used the *Dunnett*'s test. This test identifies which sample is different from the control group. When a control group did not exist, the *Tukey*'s test was performed. For a significant result when using the Kruskal-Wallis, we used the *Dunn*'s test. The latter allows testing each sample against each of the remaining samples, and verifies when they are different.

When the quantitative variables did not have a Gaussian distribution, the number of (independent) samples of the qualitative variable was determined. For two samples, the non-parametric Wilcoxon signed rank test was used. For more than 2 samples, the *Kruskal-Wallis* test was used. For a significant result, the *Dunn*'s test allowed determining which sample allows the difference.

In order to verify the independence of two categorical variables, the χ^2 test of independence was used if at least 80% of the expected frequencies were greater than 5, with *Yates*'s correction. Otherwise, the *Fisher*'s exact test was used.

After evaluating the correlation between variables, if the correlation was found to be statistically significant (p-value<0.05), linear regression models were performed.

3. Results and Discussion

3.1. Synthetic data

In Table 1, we can observe that the periodic synthetic-based volumes (Figures 5(a) and (b)) show lower $DispEn_{3D}$ values than the non-periodic synthetic-based volumes (Figures 5(c) and (d)), as expected. Since the volumes (c) and (d) are more irregular than the volumes (a) and (b), their entropy values are higher. This leads to the conclusion that $DispEn_{3D}$ has the ability to identify different irregularity degrees. In addition, volume (a) has larger variations and more gray content than volume (b). Therefore, its irregularity is higher. It should therefore lead to a higher entropy value. For similar reasons, volume (c) should lead to a higher entropy value than volumes (b) and (d). From Table 1, we observe that $DispEn_{3D}$ has the ability to differentiate such textural behaviors.

3.2. Clinical data

As mentioned above, the MRI scans of uterine fibroids were assessed using $MDispEn_{3D}$. For this work, 6 scale factors were studied and used in the computation of the θ score (see Equation 7).

Table 2
Correlation coefficient (ρ) and p-value (* means significant value) between the entropy values (scale factor $\tau = 1$ and θ) and the fibroid characteristics (size, volume, and ADC).

Variables	$\tau = 1$		θ	
	ρ	p-value	ρ	p-value
Size	−0.484	$1.21 \times 10^{-8*}$	−0.498	$4.12 \times 10^{-9*}$
Volume	−0.390	$6.14 \times 10^{-5*}$	−0.452	$2.34 \times 10^{-6*}$
ADC	−0.281	0.01^{*}	−0.077	0.46

Figure 8 shows the mean and standard deviation (SD) of the entropy values obtained for our dataset for each scale factor at D0, D10, and M6. We observe increasing entropy values with scale factors. This is true for entropy values computed at D0, D10, and M6. This can be explained by the fact that, when increasing the scale factor, the degree of down-sampling increases, and therefore, the resulting samples become less similar between each other. Given the lower similarity between samples, a more irregular down-sampled volume is obtained. When volumes are more irregular, the entropy is expected to be higher. Hence, in Figure 8, the entropy value is higher for larger scale factors since the irregularity increases with the down-sampling procedure.

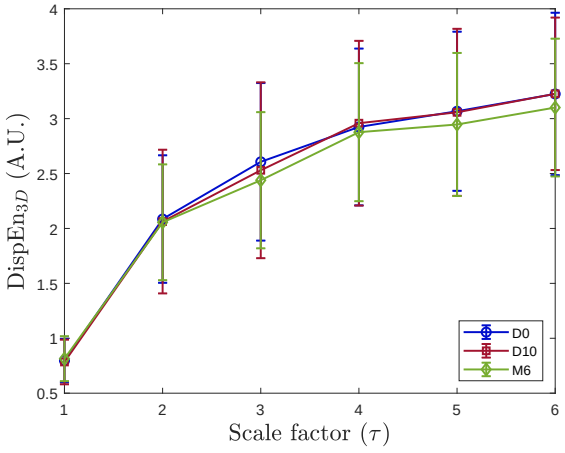

Figure 8: Mean and standard deviation values of $MDispEn_{3D}$ for D0, D10, and M6, for $c = 5$, $\mathbf{m} = [2, 2, 2]$, and $1 \leq \tau \leq 6$.

Afterwards, we studied the possible correlation between the 30 variables. As shown in Table 2, significant inverse correlations were found between $DispEn_{3D}$ value (at scale factor $\tau = 1$ and θ) and the fibroid size, between $DispEn_{3D}$ values and fibroid volume, and between $DispEn_{3D}$ at scale factor $\tau = 1$ and the ADC variable, for the periods D0, D10, and M6. These results are interesting as they reveal a direct relation between entropy values and the size and volume of the fibroid and, therefore, the evolution of the patient response to treatment.

Moreover, an inverse correlation was found between $DispEn_{3D}$ values (at scale factor $\tau = 1$ and θ) and the SSS

score at M6: coefficient of -0.459 and a significant p-value of 8.16×10^{-3} for DispEn_{3D} at $\tau = 1$, and a coefficient of -0.488 and a significance of 4.60×10^{-3} for the θ score. As mentioned above, the SSS score is obtained using surveys to assess the severity of the symptoms. Our results show that, the higher the SSS score, the lower the DispEn_{3D} values at scale factor $\tau = 1$ or θ. DispEn_{3D} and its multiscale version therefore allow to objectively quantify the severity of the symptoms.

A positive correlation between the patients age and the relative difference of DispEn_{3D} (between D0 and M6) for $\tau = 1$ was also found to be significant with a confidence of 99% ($\rho = 0.43$ and $\alpha = 8.39 \times 10^{-3}$): for older patients a higher relative difference of entropy values is observed.

As mentioned above, when significant correlations were found between variables, we proceeded to model linear regressions. We thus obtained the following linear expression:

$$y_1 = 1.07 - 0.04 \times x_1, \tag{11}$$

where y_1 represents the DispEn_{3D} entropy value at scale factor $\tau = 1$, and x_1 represents the size of the fibroma (size of the major axis of the ROI), both regardless the period, as shown in Figure 9. Nearly 28% of the variance is expressed by this regression model.

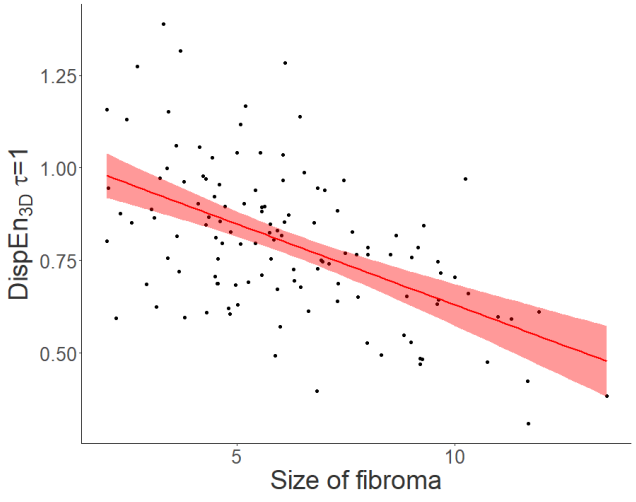

Figure 9: Linear regression between DispEn_{3D} at scale factor $\tau = 1$ using the size of the major axis of the fibroid.

A linear regression between θ and the size of the fibroma was also found:

$$y_2 = 18.81 - 0.70 \times x_2, \tag{12}$$

where y_2 represents the θ score and x_2 represents the size of the fibroma. Both variables were studied independently of the time instant (D0, D10, or M6).

Based on the relationship between the texture analysis and the fibroid major axis sizes, the evolution at M6 of fibroid size was modeled using DispEn_{3D} at scale factor $\tau = 1$ and at D0 according to the following expression:

$$\log(y_3) = 2.62 - 0.06 \times x_3, \tag{13}$$

where y_3 represents the size of fibroma at M6, and x_3 corresponds to the θ value at D0.

We also found a similar equation for $\tau = 1$ at D0:

$$\log(y_4) = 2.54 - 1.03 \times x_4, \tag{14}$$

where y_4 represents the size of fibroma at M6 and x_4 corresponds to the DispEn_{3D} value at scale factor $\tau = 1$, at D0. This model explains almost 28.0% of the variance. Multiscale entropy, using the θ score, allows explaining slightly more variance (30.0% against 28.0%), see Figure 10.

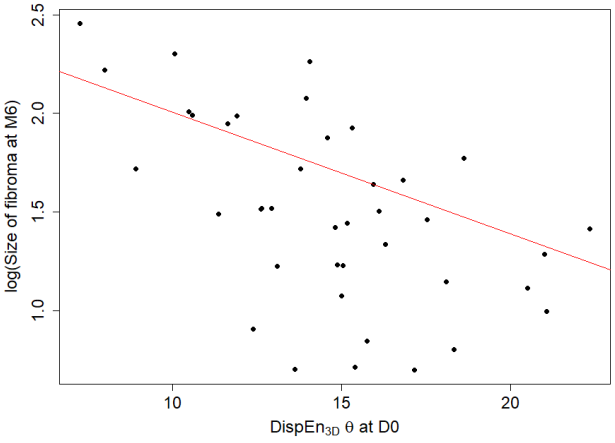

Figure 10: Linear regression explaining the size of fibroid at M6 using the θ score at D0.

Figure 11 shows the linear regression between DispEn_{3D} at $\tau = 1$ and the volume of the fibroid, regardless of the time period:

$$y_5 = 0.90 - (7.2 \times 10^{-4}) \times x_5, \tag{15}$$

where y_5 represents DispEn_{3D} at scale factor $\tau = 1$ and x_5 represents the volume of the fibroid at any period. A negative coefficient was found for this model, which was able to explain 25% of the variance. Even though size and volume are related, the size actually allows to obtain a slightly better value of explained variance.

A similar equation was found for θ and the volume of the fibroid independently of the time period:

$$y_6 = 16.23 - 0.01 \times x_6, \tag{16}$$

where y_6 represents the relative difference of θ (see Equation 7) between D0 and M6, and x_6 represents the volume of the fibroid.

The evolution of the texture (DispEn_{3D} at scale factor $\tau = 1$) between D0 and M6 was also determined using the patient age:

$$y_7 = -1.13 - 0.03 \times x_7, \tag{17}$$

where y_7 corresponds to the relative difference of DispEn_{3D} at $\tau = 1$ between M6 and D0 (see Equation 9) and x_7 represents the age of the patient.

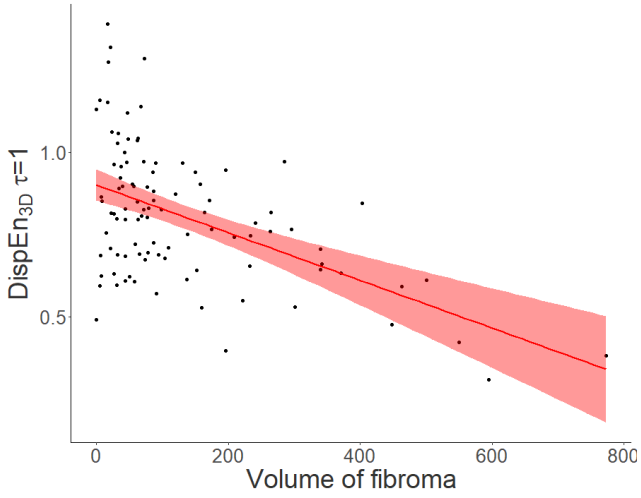

Figure 11: Linear regression between DispEn_{3D} at scale factor $\tau = 1$ and the fibroid volume.

A positive correlation between the age of the patient and the evolution of DispEn_{3D} at scale factor $\tau = 1$ between D0 and M6 was found with a p-value of 0.01, see Figure 12. This means that older patients are expected to have higher positive evolution of texture, i.e., the relative difference between $DispEn_{3D}$ values at D0 and M6 is expected to increase. This can be explained by the fact that older patients may have more often calcified fibroids, and the cessation of blood supply may result in a more significant change in texture than in younger patients. In fact, calcifications are present during the terminal phases of hyaline degeneration [24].

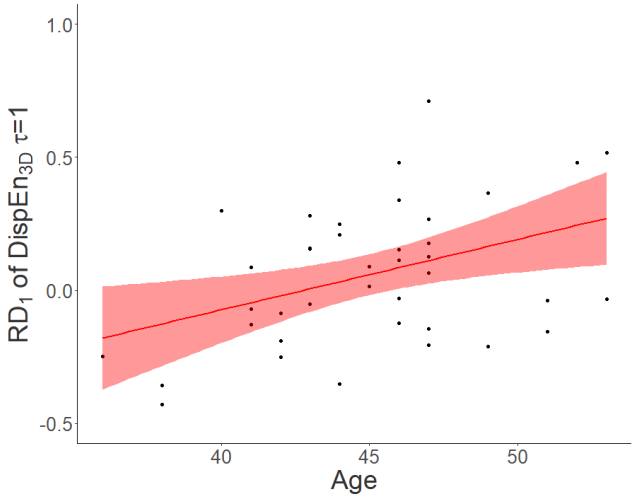

Figure 12: Linear regression between $RD_1(DispEn_{3D,\tau=1})$ and the age of the patient.

A linear regression between DispEn_{3D} at scale factor $\tau = 1$ and the SSS score, at M6, was also found:

$$y_8 = 0.09 - 0.01 \times x_8, \tag{18}$$

where y_8 represents DispEn_{3D} at scale factor $\tau = 1$ and at M6, and x_8 is the SSS score at M6.

Eq.	Variable x	Variable y	R^2	p-value
11	Size	$\tau = 1$	0.280	1.58×10^{-10}
12	Size	θ	0.251	1.86×10^{-9}
13	θ at D0	Size at M6	0.300	1.48×10^{-4}
14	τ=1 at D0	Size at M6	0.280	2.67×10^{-4}
15	Volume	τ=1	0.252	6.29×10^{-8}
16	Volume	θ	0.239	1.74×10^{-7}
17	Age	RD_1 ($\tau = 1$)	0.142	9.66×10^{-3}
18	SSS at M6	τ=1 at M6	0.161	0.01
19	SSS at M6	θ at M6	0.108	0.04

Table 3
R^2 and p-value of linear regressions obtained, equations 11 to 19.

In Figure 13 we observe that the lower the SSS score, the higher the DispEn_{3D} values, for a 98% confidence level. This relationship shows that it is possible to quantify *objectively* the SSS score.

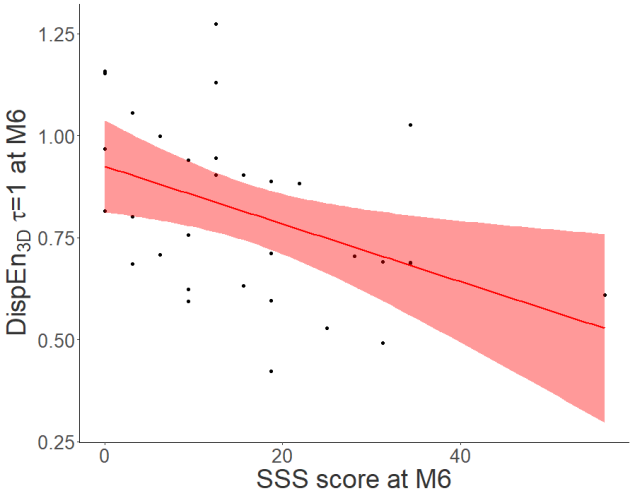

Figure 13: Linear regression between DispEn_{3D} at scale factor $\tau = 1$ and the SSS score, both at M6.

Similarly, the θ and the SSS score, both at M6, are modeled by:

$$y_9 = 15.55 - 0.08 \times x_9, \tag{19}$$

where y_9 represents the θ variable as shown in equation 7 at M6, and x_9 represents the SSS score at M6. However, this model only explains about 11% of variance.

In table 3 we summarize the linear regression models and their R^2 coefficients as well as their p-values. As we can observe, all of the linear models were found to be statistically significant for p<0.05. Moreover, 7 out of the 9 models were statistically significant for p<0.01.

Finally, from Figure 14, we observe that the group of patients that had previous history of fibroids has a higher entropy value (scale factor $\tau = 1$). The texture of fibroids between the group of patients that had previous history of fibroids and the group that did not is statistically different (p-value= 0.02). Therefore, the texture of a fibroid before

surgery might be modified with the presence of previous history of fibroid.

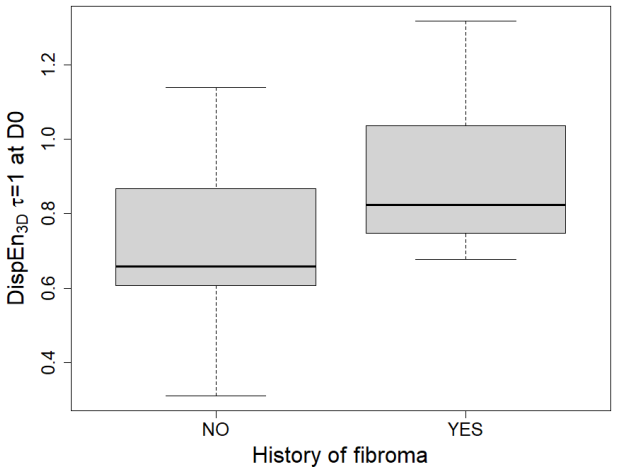

Figure 14: Boxplot representing DispEn_{3D} values (for scale factor $\tau = 1$) according to previous history of fibroid (YES) or not (NO).

4. Conclusion

In this paper we introduced the multiscale tridimensional dispersion entropy (MDispEn_{3D}). It was applied on MRI scans of uterine fibroids. One of the main results of this study is the prediction, before EFU, with a 99% confidence level, of the size of the fibroid 6 months after the embolization. Additionally, this study reveals inverse correlations between the 3D texture of uterine fibroids, using MDispEn_{3D}, and their morphological characteristics (like size and volume). These linear regressions show a confidence level higher than 99%. Moreover, the older patients show a larger positive difference in entropy values. The associated model has a confidence level higher than 99% and may be a positive indication that EFU is efficient for these patients who may have an additional benefit through this treatment.

We also have *objectively* quantified the severity of the patients symptoms using 3D texture analysis at M6. The answers to the symptom severity survey remain subjective, as sometimes the tolerance of the patient might influence her response. Texture analysis might be a good alternative to the SSS score evaluation at M6. Besides, MDispEn_{3D} may be an interesting tool to help medical doctors towards a quantification of the evolution of fibroids characteristics after EFU. It could also help in identifying if EFU is appropriate for the patient, as mentioned for the older women. If the response is negative, another treatment could be considered by the doctor.

There is still space to improve this study as it would be interesting to include patients with additional characteristics such as patients with different ethnicity, patients experiencing menopause, or other elements related to the evolution of fibroids.

CRediT authorship contribution statement

Delphine Lebret: Conceptualization of this study, Methodology, Software, Formal Analysis, Writing - Original Paper, Writing - Review and Editing.. **Andreia S. Gaudêncio:** Methodology, Software, Formal Analysis, Writing - Original Paper, Writing - Review and Editing. **Mirvana Hilal:** Supervision, Conceptualization of this study, Methodology, Formal Analysis, Writing - Review and Editing. **Sonia Saib:** Conceptualization of this study, Methodology, Resources, Writing - Review and Editing. **Rakelle Haidar:** Methodology, Software. **Michel Nonent:** Conceptualization of this study, Methodology, Resources, Writing - Review and Editing. **Anne Humeau-Heurtier:** Supervision, Conceptualization of this study, Methodology, Formal Analysis, Writing - Review and Editing.

References

[1] S. Gupta, J. Jose, I. Manyonda, Clinical presentation of fibroids, Best practice & research Clinical obstetrics & gynaecology 22 (2008) 615–626.

[2] S. Okolo, Incidence, aetiology and epidemiology of uterine fibroids, Best practice & research Clinical obstetrics & gynaecology 22 (2008) 571–588.

[3] M. G. Munro, H. O. Critchley, M. S. Broder, I. S. Fraser, for the FIGO Working Group on Menstrual Disorders, Figo classification system (palm-coein) for causes of abnormal uterine bleeding in nongravid women of reproductive age, International Journal of Gynecology & Obstetrics 113 (2011) 3–13.

[4] H. Ueda, K. Togashi, I. Konishi, M. L. Kataoka, T. Koyama, T. Fujiwara, H. Kobayashi, S. Fujii, J. Konishi, Unusual appearances of uterine leiomyomas: Mr imaging findings and their histopathologic backgrounds, RadioGraphics 19 (1999) S131–S145. PMID: 10517450.

[5] A. M. White, J. B. Spies, Uterine fibroid embolization, Techniques in Vascular and Interventional Radiology 9 (2006) 2–6.

[6] J. B. Spies, K. Coyne, N. G. Guaou, D. Boyle, K. Skyrnarz-Murphy, S. M. Gonzalvez, The ufs-qol, a new disease-specific symptom and health-related quality of life questionnaire for leiomyomata, Obstetrics & Gynecology 99 (2002) 290–300.

[7] M. Sand, R. Rosen, C. Meston, L. Brosso, The female sexual function index (fsfi) : a potential "gold standard" measure for assessing therapeutically-induced change in female sexual function, Fertility and Sterility 92 (2009) S129.

[8] C. Morel, A. Humeau-Heurtier, Multiscale permutation entropy for two-dimensional patterns, Pattern Recognition Letters 150 (2021) 139–146.

[9] M. Hilal, C. Berthin, L. Martin, H. Azami, A. Humeau-Heurtier, Bidimensional multiscale fuzzy entropy and its application to pseudoxanthoma elasticum, IEEE Transactions on Biomedical Engineering 67 (2020) 2015–2022.

[10] A. Humeau-Heurtier, Texture feature extraction methods: A survey, IEEE Access 7 (2019) 8975–9000.

[11] L. E. Virgilio da Silva, A. C. Da Silva Senra Filho, V. P. S. Fazan, J. C. Felipe, L. O. Murta, Two-dimensional sample entropy analysis of rat sural nerve aging, in: 2014 36th Annual International Conference of the IEEE Engineering in Medicine and Biology Society, 2014, pp. 3345–3348. doi:10.1109/EMBC.2014.6944339.

[12] L. E. Silva, A. C. Senra Filho, V. Fazan, J. Felipe, L. Murta, Two-dimensional sample entropy: assessing image texture through irregularity, Biomedical Physics & Engineering Express 2 (2016) 045002.

[13] C. Moore, T. Marchant, The approximate entropy concept extended to three dimensions for calibrated, single parameter structural complexity interrogation of volumetric images, Physics in Medicine & Biology 62 (2017) 6092.

[14] A. S. F. Gaudêncio, P. G. Vaz, M. Hilal, J. M. Cardoso, G. Mahé, M. Lederlin, A. Humeau-Heurtier, Three-dimensional multiscale fuzzy entropy: validation and application to idiopathic pulmonary fibrosis, IEEE journal of biomedical and health informatics 25 (2020) 100–107.

[15] A. S. Gaudêncio, P. G. Vaz, M. Hilal, G. Mahé, M. Lederlin, A. Humeau-Heurtier, J. M. Cardoso, Evaluation of covid-19 chest computed tomography: A texture analysis based on three-dimensional entropy, Biomedical Signal Processing and Control 68 (2021) 102582.

[16] M. Rostaghi, H. Azami, Dispersion entropy: A measure for time-series analysis, IEEE Signal Processing Letters 23 (2016) 610–614.

[17] H. Azami, L. E. V. da Silva, A. C. M. Omoto, A. Humeau-Heurtier, Two-dimensional dispersion entropy: An information-theoretic method for irregularity analysis of images, Signal Processing: Image Communication 75 (2019) 178–187.

[18] M. Costa, A. L. Goldberger, C.-K. Peng, Multiscale entropy analysis of complex physiologic time series, Physical Review Letters 89 (2002).

[19] S. C. G. Laboratory, Texture synthesis : Misc textures, ???? URL: https://graphics.stanford.edu/projects/texture/demo/synthesis_eero.html, accessed july 2021.

[20] L.-Y. Wei, M. Levoy, Fast texture synthesis using tree-structured vector quantization, in: Proceedings of the 27th Annual Conference on Computer Graphics and Interactive Techniques, SIGGRAPH '00, ACM Press/Addison-Wesley Publishing Co., USA, 2000, pp. 479–488. URL: https://doi.org/10.1145/344779.345009. doi:10.1145/344779.345009.

[21] H. Azami, J. Escudero, Amplitude- and fluctuation-based dispersion entropy, Entropy 20 (2018).

[22] W. Chen, J. Zhuang, W. Yu, Z. Wang, Measuring complexity using fuzzyen, apen, and sampen, Medical Engineering & Physics 31 (2009) 61–68.

[23] M. Labriffe, L.-M. Leiber, Diffusion, cartographie adc, effet t2 en irm cérébrale : kézaco, Journal d'imagerie diagnostique et interventionnelle 2 (2019) 289–293.

[24] M. Zulfiqar, A. Shetty, R. Tsai, M.-H. Gagnon, D. M. Balfe, V. M. Mellnick, Diagnostic approach to benign and malignant calcifications in the abdomen and pelvis, RadioGraphics 40 (2020) 731–753. PMID: 32302263.